



Improving Seismic Activity Monitoring with AI-Driven Earthquake Parameters using Short-to-Long-Term Average Analysis

Mukesh Kumar Gupta¹, Brijesh Kumar²

¹Computer Science and Engineering Department Manav Rachna International Institute of Research and Studies (MRIIRS), Faridabad, INDIA
mukeshgupta@dce.ac.in

 <https://orcid.org/0000-0001-6188-5998>

²Computer Science and Engineering Department Manav Rachna International Institute of Research and Studies (MRIIRS), Faridabad, INDIA
brijesh.fet@mriu.edu.in

 <https://orcid.org/0000-0002-6237-5970>

ARTICLE INFO

ABSTRACT

Received: 30 Dec 2024

Revised: 05 Feb 2025

Accepted: 25 Feb 2025

Earthquake Early Warning Systems (EEWS) play a crucial role in mitigating earthquake impacts by providing timely alerts to affected regions. This study explores an AI-driven algorithm leveraging seismic trace migration and stacking to enhance the detection of seismic events. By analysing data from a temporary network in a volcanically active region, the algorithm identified optimal detection parameters, achieving a remarkable 94% detection rate, significantly outperforming conventional systems. Additionally, it identified 209 previously undetected events while maintaining a lower false detection rate of 25%, compared to the system's 40%. Key innovations include the application of Kurtosis functions and short-to-long-term average variations, enabling precise detection of seismic traces. The method demonstrated efficacy in analysing large swarms of low-magnitude events with short inter-event times, making it especially suitable for monitoring regions with complex seismic activities, such as fluid injection, drilling, and volcanic areas. Despite its computational intensity, the algorithm's scalability and accuracy present a promising advancement in real-time seismic monitoring. Empirical tests affirm the utility of small, representative data subsets for fine-tuning detection parameters, reinforcing the system's robustness. This approach underscores the potential of AI-driven methods in advancing seismology, improving early warning systems, and contributing to disaster risk reduction globally.

Keywords: Earthquake early warning (EEW); Earthquake prediction; Machine learning; Numerical solutions; Time-series analysis; Seismicity; Seismology.

1. INTRODUCTION

Modern instrumentation technology makes it possible to install dense seismological arrays at a reasonable cost and record seismic data permanently or semi-permanently. Data analysis and evaluation must be automated, dependable, and computationally efficient due to the ever-increasing volume of data. Many seismic applications rely on the detection of seismic events, with the challenging but desirable goal of creating an automatic event catalogue that is as comprehensive as possible while having a small number of "false" events that must be eliminated. False events can be hard to spot and frequently require laborious manual examination of multiple seismic traces. The most common seismic event detectors are usually single station phase onset detection, phase identification and association, and the final event location and quality evaluation [1]. P- and/or S-phase onsets are therefore be successfully detected and identified in order for an event to be detected. Phase detectors frequently employ changes in seismic trace characteristics, like amplitude, envelope, or power, to record distinctive shifts in particle motion [2]. These characteristics should ideally remain flat in other locations and generate amplitude peaks at the beginning of energy bursts. A short-term average to long-term average ratio (STA/LTA) is a common example of a phase detector, as well as variants of the m [3]. It is shown in the given below figure 1.

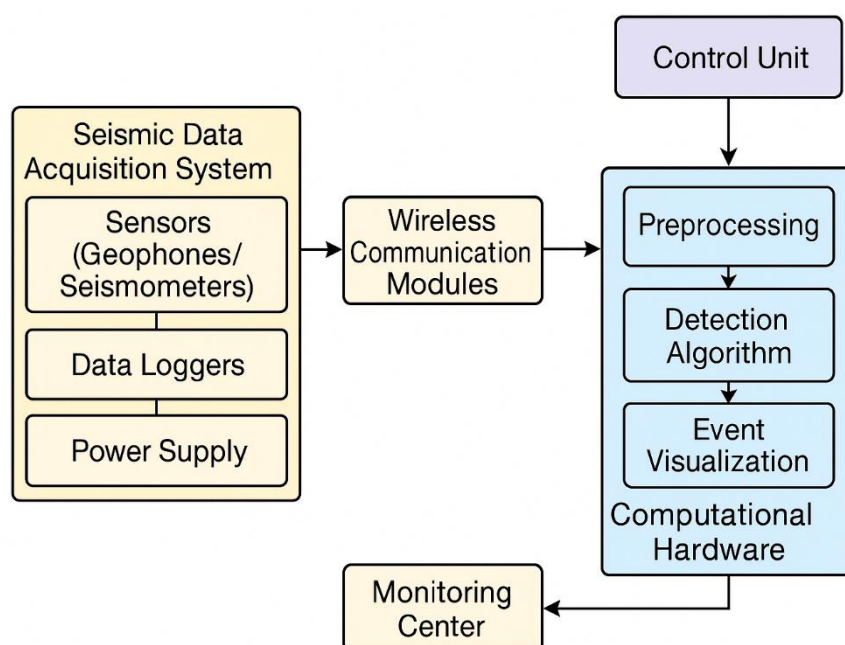


Figure 1. Block Diagram for Seismic Data Preprocessing

2. DATABASE AND METHODOLOGY

The methodology prioritizes the largest event at each time step, potentially missing smaller overlapping events. Four primary steps can be distinguished in migration and stack-based detection.

(1) Pre-processing of the trace, which typically consists of frequency filtering the seismic data and selecting an attribute function to maximize the desired signals and reduce noise. Instead of emphasizing the maximum amplitude, we compare stacking various nonlinear characteristics of the waveform data (Kurtosis, STA/LTA), which indicate the beginning of an incoming phase.

(2) Migration of the pre-processed traces and stacking. S-wave and 1-D P-wave velocity models have both been used in earlier research [4]. P-wave velocity model in three dimensions. The travel time look-up tables were calculated in 2014. We employ a 3-D P- and S-wave velocity model based on it [5], so that we created using our own local earthquake tomography.

(3) Finding peak amplitudes in the stacked data and locating them. We evaluate hypocentre uncertainty and identify events by scanning a reduced 1-D stack [6]. An algorithm for adaptive threshold search has been put into place to enhance detection, particularly for events with brief inter-event intervals.

(4) During processing of events, we examine the number of phase arrivals with enough S/N to evaluate the quality of an event and use automatically selected S-wave amplitudes to estimate local event magnitudes. We finally used an iterative resampling technique.

2.1 Trace pre-processing

Coherency in the stack is ensured by bandpass filtering the raw seismic traces to the frequency band that improves the S/N in the attribute function and generates a constant signal strength over all source-receiver distances. The frequency range utilized for manual phase picking may differ from this one [7]. We found that the P- and S-signals in our test data set had a range of spectra. The highly inhomogeneous velocity structure, source mechanisms, and the space- and time-varying noise field all contribute to the observed spectra. For simplicity, we define optimal lower and upper bounds f_{lo} and f_{hi} based on the range of observed dominant frequencies and the S/N of the stacked filtered traces [8]. We also choose constant frequency bands. The frequency ranges selected are 2–15 Hz for S (horizontal) and 2–30 Hz for P (vertical) traces. We anticipate that most seismic signals will reach a station with sub-vertical incidence due to the strong velocity gradient in the top few kilometres of the Icelandic crust; as a result, P-energy will

be primarily on the vertical component and S-wave energy will be on the horizontal components. Therefore, we use the vertical component as the P-trace and use $\sqrt{E_2 + N_2}$ to calculate an S-trace from the two horizontal components, E and N [9]. To emphasize the P- and S-phase onsets, respectively, and raise S/N, attribute functions are applied to both P- and S-traces. Reliable at various S/N ratios, the STA/LTA is a strong option for a range of seismic signals. It works reliably at different S/N ratios. It can be defined as

$$\frac{STA}{LTA}(t) = \frac{N_L \sum_{i=1}^{N_S} |y(t + i \, dt)|}{N_S \sum_{i=1}^{N_L} |y(t - i \, dt)|} \quad (1)$$

STA and LTA in equation (1) can be used to define it, where dt is the sampling rate and $y(t)$ is the frequency filtered trace at the specified station. In the STA and LTA time windows, the number of points is denoted by N_L and N_S , respectively. Depending on the frequency content of the signal under analysis, the time windows' ideal lengths vary. It proposes that for their adaptive STA/LTA filter, the LTA window is nine times longer than the STA window, and the STA window includes three "cycles" (6 zero-crossings) of the signal. For P and S signals, respectively, we select 0.1s (STA) and 1s (LTA), and for S signals, 0.2s (STA) and 1s (LTA). These windows are comparatively brief in relation to the signals' observed frequency content, in order to increase the STA/LTA's variability. $io(t - idt) - \mu t]4K(t), (2) Nk \sigma t$ is the definition of the Kurtosis function, a statistical measure of the ratio of a distribution's tail to its width, where μt and σt are the data's mean and standard deviation within a time window of Nk points. Three is the Kurtosis value for a univariate normal distribution; higher values denote a spiked distribution. Kurtosis values greater than three are regarded as seismic signals, presumed to be random, independent, and normally distributed seismic noise [10]. The Kurtosis function's positive gradient was also used to increase the detection timing accuracy.

A traditional single trace picker's detection results are compared to ours, so the system detection software [11]. We also evaluate and contrast the same attribute function with the other three attribute functions that are utilized in the system software. A forward difference filter and a high-pass filter are used in the system software to filter traces. This is followed by an STA/STA, or STA/LTA with two equally long-time windows, which we call the system attribute function or STA / STA (grad). A 0.2s window is used to calculate the system attribute function for both STA windows. But take note that there are additional steps involved in system detection, like Table 1. Figure 2 displays sample traces, and Table 1 summarizes the parameters selected for the various attribute functions [12]. Around the selected phase onsets, the STA/LTA generates fairly broad, symmetrical signals, whereas the Kurtosis function first increases sharply before gradually declining. While the slowly decaying tail is eliminated by the Kurtosis gradient, several peaks may still form.

Table 1. Trace pre-processing, Migration and detection parameters for an event detection.

Attribute	f_{lo} [Hz]	f_{hi} [Hz]	STA [s]	LTA [s]
STA/LTA	2	30(P), 15(S)	0.1(P), 0.2(S)	1
STA/STA (grad)	2	–	0.2	–
Kurtosis	2	30(P), 15(S)	–	1
Grad (kurt.)	2	30(P), 15(S)	–	1

Note, however, that the system detection includes further steps, such as phase association and selection, which influence the outcome of the detection.

2.2 Migration and stack

The migration and stacking process involves stacking attribute traces time shifted using travel time tables from 3-D velocity models. The models used for this study are in essence although with a higher resolution due to the denser station coverage [13].

The stack is then defined as the normalized sum of all time shifted traces where f_n is the chosen attribute function for the n th component and τ_{kl} the travel time estimate from the k th grid point to the l th station. The travel time tables are calculated with the time 3d finite difference algorithm. The two stacked components are the P- and S-traces.

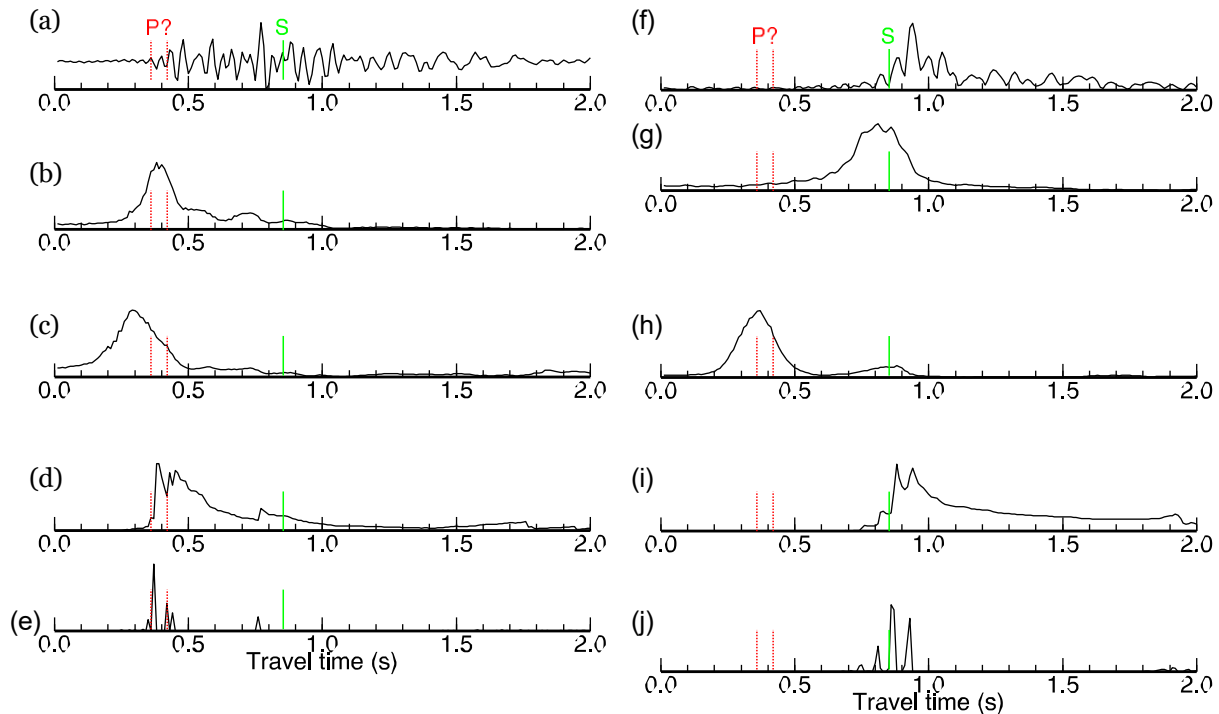


Figure 2. Left: Bandpass filtered (2–30 Hz) and normalized vertical component seismic trace (a) and derived attribute traces (b–e). Right: Bandpass filtered (2–15 Hz) and normalized S-component trace (f), that is, Euclidean norm of horizontal components, and derived attribute traces (g–j). Attributes are: STA/LTA (b,g), STA/STA(grad) (c,h), Kurtosis (d,i) and grad(kurt) (e,j). The signal was recorded at station lha after event 1. Potential first arriving P- and S-picks are marked with red and green vertical lines, respectively. Time is travel time, that is, relative to estimated event origin time.

Travel timetables from velocity models are used to stack attribute traces time shifted during the migration and stacking process. We combine manual travel time selections stations in the study area with P- and S-wave velocity models from a nearby earthquake tomography study [14]. In essence, the models employed in this investigation are comparable to those put forth, but because of the denser station coverage, it has a higher resolution. Then, the stack is defined as the normalized sum of all time shifted traces, where τ_{kl} is the estimated travel time up to the l th station and function (n) is the selected attribute function for the n th component. The time 3d finite difference algorithm is used to compute the travel time tables [15]. The P- and S-traces are the two stacked components.

The length of the stacking window is directly related to the maximum travel-time between two diagonally spaced grid points and given by with x the constant grid sampling, V_{min} the slowest velocity in the model and mtw a constant user defined factor.

2.3 Event detection

Similar to other algorithms, we store only the maximum stack amplitude at each time step that is, reducing the stack to a function of time. Another parameter l (0 to 1) is defined to estimate the hypocentre and origin time uncertainty. We set the origin time uncertainty for each event (max_k) equal to the time interval (T_u) where $S_m > lmax_k$. Hypocentre uncertainty is then estimated as the standard deviation of X_m within T_u [16].

In order to achieve reasonable spatial resolution in near real-time, we adopt an iterative detection and resampling procedure. The length of the stacking window is directly related to the maximum travel time between two diagonally spaced grid points and given by with x the constant grid sampling, V_{min} the slowest velocity in the model and mtw a constant user defined factor [17] [18]. To identify time segments and grid portions that might contain one or more

events, a first low-resolution stack is calculated. The stack is recalculated at greater spatial resolution in the subsequent iterations.

However, in the absence of a coherent signal, we find that consecutive points in S_m randomly correspond to very different locations X_m [19]. We only combine the energy from the biggest event in the region at a specific moment since we only analyse the maximum stack at each time step. Thus, each S_m peak is thought to correspond to a single event. Although event peaks in S_m get wider with lower sampling, this isn't always the case at coarse spatial and, consequently, low temporal sampling. Figure 2 illustrates how the maximum stack function S_m 's resolution decreases as grid sampling decreases.

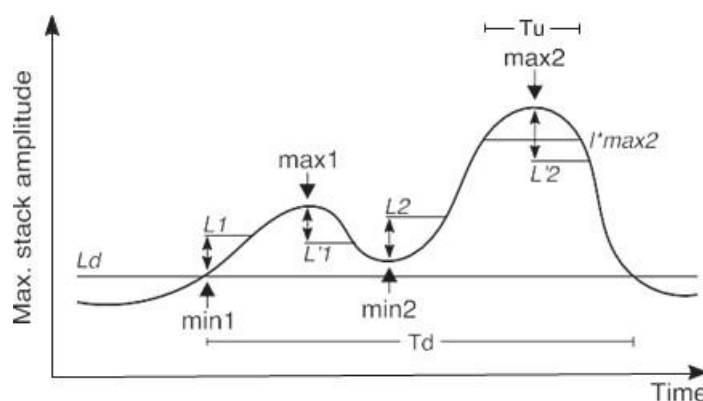


Figure 3. Adaptive local maximum detection procedure to detect small local peaks in the maximum stack function S_m , each representing a possible event. T_d marks the detection interval where the procedure is active. Local detection thresholds L_k and L'_k are defined based on the preceding trough \min_k or peak \max_k to detect the next peak \max_{k+1} or trough \min_{k+1} , respectively. For each peak, an uncertainty interval T_u is defined to calculate origin time and hypocentre uncertainty.

When S_m is higher than a user-defined detection threshold, L_d , an event is detected. There are two ways to characterize the detection threshold: constant and time varying (when there are different noise levels present). By computing a mean stack time-series with N grid points. A moving average over time is indicated by the brackets [20]. The time varying detection threshold is then equal to the moving average of S_u over time plus a constant value [21]. The averaging window length that we propose is greater than a number of event peaks. It is frequently not possible to differentiate between two closely spaced local maxima in S_m using one of the aforementioned thresholds; instead, the constant term should be marginally greater than the average variation of S_m around [22]. Defining peaks in S_m at low spatial resolution may merge if inter event times are brief because of the stacking window approach, which makes them wider. To find as many peaks as we can, we look for several local maxima during the time interval (T_d) when the stack surpasses the detection threshold. Depending on the preceding trough (or peak), we establish a local detection threshold within T_d for every peak (and trough). To achieve this, we established a fixed peak-to-trough ratio (d) and the subsequent local detection threshold. This adaptive detection keeps going until the detection window T_d is over. These are the adjusted local detection thresholds, L_1 and L_2 . Another parameter, l , is defined to estimate the value between 0 and 1 [23].

2.4 Local magnitude estimation

We define our own local magnitude scale and calibrate it to the system. A linear relationship between the local magnitude ML , the log of the epi-central distance (D), and the log of the S-wave amplitude (A) of an event is assumed, where α , β , and γ are constants determined for each individual station using linear regression.

An estimate of event magnitudes is helpful to fine-tune algorithm parameters and to assess our algorithm's performance with meaningful statistics. The system local magnitude is calibrated to our own local magnitude scale. The local magnitude (ML), log of the epi-central distance (D), and log of the S-wave amplitude (A) of an event are assumed to have a linear relationship, where linear regression is used to determine the constants α , β , and γ for each individual station. The maximum zero-to-peak amplitude of the transverse component within a projected arrival time

window is used to automatically estimate the S-wave amplitudes [24]. In order to prevent P-wave contamination in the S-wave window, we opt for the transverse component. After detection, it is computed by rotating the horizontal components in relation to the estimated event location. To identify the presence of the corresponding phase, arrival time windows for the P- and S-phases are established. In relation to the anticipated travel time τ_{kl} , the lower time boundary t_1 is provided with v_{source} the velocity at the estimated event location, c a constant estimate of the relative velocity error (0 to 1), and δ a spatially uniform hypocentre uncertainty from the event detection. Although δ and c have opposite signs, the upper boundary t_2 has the same form. We assume all travel time residuals τ_i in order to determine an appropriate value for c .

The time windows are typically long enough (roughly 0–5 seconds, depending on source-receiver distance) and skewed towards later times so that they reliably cover the maximum S-wave amplitude, even though the maximum S-wave amplitude frequently arrives later than the phase onset. The identified P-phases can be used to define event quality, such as by counting toward the total number of observed phase arrivals, but they do not aid in magnitude estimation. Using the system catalogue to enter the local magnitudes, event locations, and S-wave amplitudes, the regression parameters α , β , and γ are established. Because of either a lack of detected S-phases or inaccurately estimated S-amplitudes, the parameters may not be well determined for some stations. Those stations are rejected. The magnitudes of each detected event are estimated for each of the remaining stations. The median of all an event's station-specific magnitudes is then used to determine its local magnitude. This rapidly produces imprecise estimates for local magnitudes, much like the Richter scale, but it ignores any kind of radiation pattern because of the event's source mechanism [25].

3. APPLICATION TO MICRO EARTHQUAKE DATA FROM A REGION

Region associated geothermal fields are currently exploited for geothermal energy in several locations, including nine active reinjection wells. The geology consists of hyaloclastite formations topping the base of the central volcano and containing elongated lens-like interglacial lava series and a postglacial lava layer.

In an attempt to better characterize the geometry and potential of the geothermal reservoir, a high-density seismic network with broad-band (120s) sensors. All data were recorded with a sampling rate of 100Hz. The volcanic system is the most noticeable formation. There are currently active reinjection wells where its associated geothermal fields are being used to generate geothermal energy. Over the course of four years, a high-density seismic network comprising twenty seismological stations equipped with broad-band (120s) sensors. All of the stations were operational at the same time [26] [27].

The seismicity is partly due to the plate-tectonic setting but a large number of small magnitude events are related to drilling and re-injection of waste water at the production sites. The remaining 97 events were found using the system automatic detection software with the data from the enhanced temporary network followed by manual picking.

Although the plate-tectonic setting contributes to some of the seismicity, drilling and waste water re-injection at production sites are responsible for a significant number of small magnitude events. Time and place have a significant impact on noise levels. Events of various kinds are seen, some of which have ambiguous P and/or S phase arrivals. We used data spanning six days to test our algorithm. To encompass various event clusters across the study region, we chose non-contiguous days (2011 November 2/3, 2012 March 2/19, and 2012 July 7/8). Earthquake swarms in November 2011 and July 2012 showed inter event times as short as a few seconds. For those days, a total of 234 manually selected events were known. These are referred to as "system" events. 137 of them were captured by the permanent network. We calibrate our own local magnitude scale using the event magnitudes that are listed in Iceland's public earthquake catalogue. The system automatic detection software was used to locate the remaining 97 events using the enhanced temporary network data, which was then manually selected. During this process, we determined that several events had been overlooked and that roughly 40% of the events that the system software automatically detected were false. Low S/N and brief inter event intervals during swarms were primarily blamed for the overlapping of phases from various events.

4. RESULTS

$t = 0.12s$ and $t_w = 0.58s$ are the results of a second iteration that is conducted at 1km sampling. The final detection is performed using $d = 0.75$ and $l = 0.95$ after the second iteration stack has been calculated. This allows for the distinction of multiple event peaks within each time interval and yields reasonable uncertainty values. Following the second iteration, the maximum stack function for the various attribute functions. However, the stack was generated with fewer stations and a smaller search volume for every event (determined by its location uncertainty). We categorized the automatically detected events as either "true" or "false" events for the purposes of the analysis that follows. If an event is locatable and at least four phases are discernible, it is deemed true. Every other occurrence is regarded as untrue. While generally strong, these standards are not perfect. Therefore, in addition to real events of low magnitude that are too weak to be recognized as true events, false events can also be caused by noise bursts that coincidentally stack coherently. Events with an origin time of less than two seconds (no multiple matches) are referred to as "matching" events when comparing event catalogues [28].

4.1 Comparison of attribute functions and completeness of detected events

In order to test the algorithm, we look at both the number of false events generated and the completeness, and the number of missed events compared to a "complete" event catalogue. True events identified by various attribute functions were combined with manually selected events to create a "complete" catalogue of 480 true events. By computing the ratio of missed events to false events, the entire catalogue is used to evaluate our algorithm's detection performance in relation to the input attribute function and the selection of the detection threshold. Notwithstanding the fact that we did not manually verify every event, we regard all events above the dashed line as false events in accordance with our definition of the complete catalogue. The ideal detection threshold is 7. A low percentage of missed events at low detection thresholds and few false events at high thresholds are the outcomes of the STA/LTA, Kurtosis, and the positive gradient of the Kurtosis. The Kurtosis function produces slightly better results.

Less than 10% of all known events are missed by the ideal detection threshold, which produces roughly 75% true events. In contrast, the system attribute function (STA/STA (grad)) has a less defined knee and a much flatter curve. This could make it more challenging to adjust the detection threshold for best results. It should be noted that the system detection software's phase detection is intended to produce a large number of detections, and that a phase association procedure is then implemented to get rid of false phase detections. Therefore, our findings show the performance of the system detection software's attribute function (i.e., rather than the software's overall performance) and phase detection in relation to our algorithm that is based on migration, further lowering the detection threshold than what is depicted in Figure 4 quickly raises the cost of false events while not achieving less than roughly 5% of missed events. The cause is a small number of events from the entire catalogue that take place in close proximity (both in time and space) to larger events and were only discovered by hand-examining the data; neither the migration nor the system algorithm were able to identify them [29].

5. Discussion

Event detection via migration and stack techniques, unlike methods relying solely on phase picking from a single trace, mandates a velocity model of the subsurface for the detection process. This approach inherently assumes that the supplied velocity model, and the subsequent migration or backpropagation algorithms, adequately mirror the actual physical conditions and seismic wave propagation. Utilizing travel time residuals, we've gauged the maximum relative error of our velocity model at 5 percent. Importantly, migration and stack techniques primarily respond to portions of the velocity model that influence the predicted travel times, specifically those cells traversed by seismic rays. Analysing stacks at varied spatial resolutions, we've observed a sensitivity to velocity anomalies exceeding 1 km. Our wave field simplification focuses exclusively on first-arriving P and S waves, anticipating these to create the most pronounced peaks in the attribute function. Therefore, phenomena like multi pathing and surface waves are disregarded. Furthermore, we did not correct for distance-amplitude decay; such correction consistently degraded the stacked results by amplifying noise originating from distant recording stations. A more sophisticated wave field modelling could necessitate a more comprehensive understanding of the velocity structure to yield an advantage.

It's crucial to consider the combined error in travel time resulting from both the velocity model and the back-propagation stage when we're stacking the attribute function we've selected. Our observations suggest that stacking

the highest amplitude within a user-specified temporal window – which, at its core, applies a maximum value filter to the incoming data – effectively addresses travel time discrepancies. Another approach involves substituting the peaks observed in the attribute function traces with Gaussian functions. These Gaussians can have either a fixed or fitted width, and this replacement often enhances constructive stacking, leading to more precise event localization. The Gaussian functions introduced in this manner can provide an estimate of the arrival time uncertainty, which can then be used to calculate origin time and location uncertainties following the stacking process. However, one must also set a threshold to identify these attribute function peaks, which causes data below the set threshold to be dismissed; in essence, this introduces a method of phase detection.

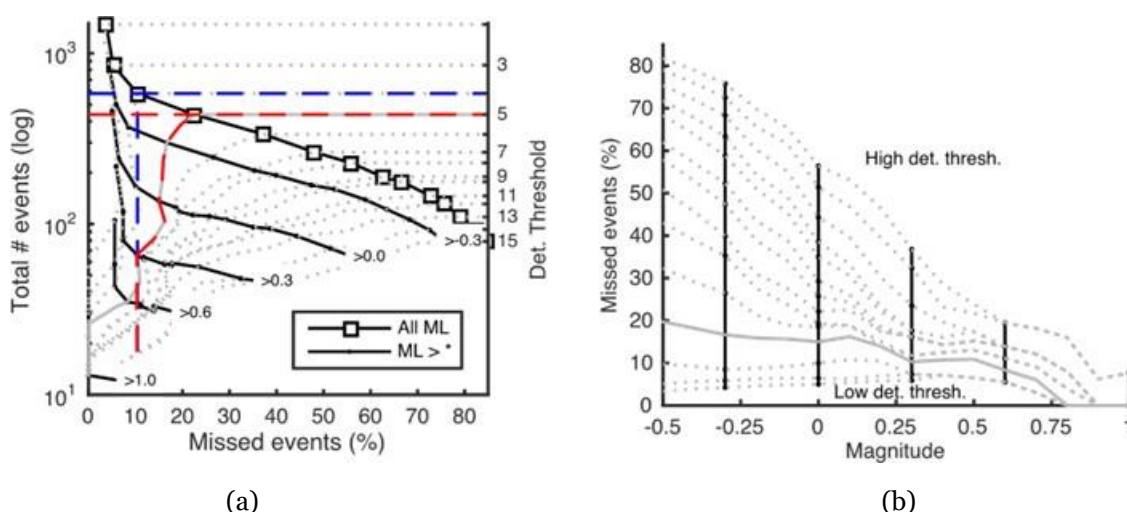


Figure 4. (a) General trade-off between a low number of detected events and a low percentage of missed events for the Kurtosis attribute function and various magnitude ranges. Black squares show all detections for an increasing detection threshold from left to right. Black solid lines with dots represent trade-off curves for events above different magnitude thresholds. Points connected by grey dotted lines belong to the same detection threshold. Two scenarios are highlighted by the blue and red lines. (b) Same data and colour codes as in (a), but re-organized as percentage of missed events above a given magnitude for different detection thresholds.

Data pre-processing involves selecting a frequency band and an attribute function. Our choice of broad, constant frequency bands stems from observing the dominant frequencies present in the P- and S-phases. This wide definition appears appropriate for the automated detection of a diverse range of events in a seismically active region like Iceland. While we haven't looked into adaptive frequency filters, we believe that shorter bands could reduce signal strength within the attribute function, the stack, or both [30].

5.1 Frequency bands and attribute functions

We observed comparable performance across three attribute functions evaluated: (i) the STA/LTA, (ii) Kurtosis, and (iii) the gradient of the Kurtosis. The system function, designed to maximize phase detection, couldn't be tuned to perform on par with the other three [31]. Possible reasons include the use of a high-pass filter instead of a band-pass filter, and the higher variability in the STA/STA values compared to STA/LTA values. Although these results suggest similar effectiveness among different attribute functions, each function identified a slightly unique set of events. Lacking further analysis of the detected events, we can only infer that a particular attribute function might be advantageous for pinpointing specific types of events. We did not find significant improvements in hypocentre estimates, with the Kurtosis demonstrating slightly better detection statistics [32].

5.2 Runtime improvements and impacts

The crucial element in developing a real-time, migration-based detection algorithm is runtime. Runtime for a finite difference grid is proportional to the cube of grid points. This means that grid size and sampling heavily affect the runtime. The grid size is often determined by the study area's dimensions and not easily altered. Practically, the

spatial grid must be constructed to encompass all required stations and desired seismic activity. However, regional or tele seismic events might be located inaccurately within the model. These events sometimes appear close to the model boundaries. We, therefore, recommend removing events from a "critical zone" along the model boundaries [33].

Grid sampling influences the spatial and temporal resolution of detection. So we proposed an iterative up-sampling approach to reduce computation time. Based on our implementation, we offer the following practical insights: (i) events missed during the initial, coarse iteration are irrecoverable in later iterations; (ii) the high location uncertainty in a coarse-grid iteration might render the defined time interval and sub-volumes unsuitable for later iterations; (iii) Parameters that tie temporal sampling to spatial sampling, such as the stacking window and time step multipliers, are essential to prevent spatial resolution loss [34]. This is effectively transformed into a loss of temporal resolution ("smearing" event peaks over time). When using an iterative method, selecting the initial iteration parameters—detection threshold, grid resizing, time interval for subsequent iterations, time step, and stacking window lengths—is critical for successful detection. In our experience, more than two iterations generally complicate things without further gain [35].

We also observed that stacking only the nearest stations at each grid point can enhance the stack for low-magnitude events while simultaneously decreasing runtime. This enables each point within the 4-D stack to, in theory, include data from different areas. Therefore, when signals from several events overlap, we will only observe the stacked amplitude of the strongest event at that given time [36].

5.3 Result appraisal: magnitude estimates, completeness, and event quality

To evaluate the efficacy of any event detection algorithm (in terms of detection capability), it's critical that the detected events include a magnitude estimate. We derive our magnitude estimations from hypocentre estimations, coupled with automatically selected S-amplitude data. Refining these magnitude calculations by incorporating manually picked phase arrival times, event relocation, and the analysis of S-phase frequency content is an approach that could offer improved magnitude estimation [37]. However, the magnitude distributions we generated align well with the system data and were deemed adequate for this research. We note a small underestimation of magnitudes exceeding ML 1.2.

In the context of a seismic network, the magnitude of completeness (M_c), assessed using a frequency–magnitude diagram, denotes the magnitude threshold below which the detection of a substantial number of events becomes unreliable. Whether an event below M_c is detected depends on its location within the network, the stations available for observation, and the level of noise at nearby stations—all of which may fluctuate over time. Yet, M_c does not guarantee that all events surpassing this threshold are easily detected. Our findings reveal that the application of a migration and stacking algorithm necessitates the examination of a significant number of false events to identify all possible events. This is, based on intuition, not necessarily a property exclusive to migration and stacking, because all event detection approaches must deal with events nearing or below M_c in magnitude where detection becomes challenging due to network-specific constraints. Simultaneously, specific events went undetected because of an inability to differentiate them as two discrete events (inter-event separation measured in seconds). The magnitudes associated with these events (along with chosen detection thresholds) have a secondary effect; it is their close proximity that triggers failure within the detection algorithm. It is very likely that this issue could impede any event detection algorithm. Therefore, we contend that various factors, such as event location, wave propagation, and signal-to-noise (S/N) ratio at the receiver, impact the event's detectability, independent of its magnitude estimation. This may obfuscate the direct relationship between detection threshold and magnitude estimation – a relationship potentially prone to significant temporal and spatial variation [38].

False events in our detection outputs either originated from extraneous noise bursts – associated with environmental influences or instrumentation – or were, in fact, legitimate events, categorized incorrectly because they failed to meet our criteria, particularly relating to the count of identifiable phases. Noise bursts can impact the stack process with varying degrees of significance, dictated by the signal strength they generate within the attribute function. As a result, careful data examination is advised, together with the standard removal of noisy and/or erroneous traces to minimize false detections due to random noise bursts [39].

6. CONCLUSIVE REMARKS

Migration-based event detection presents a beneficial alternative to traditional event detection algorithms founded on single-trace phase detection. The migration process diminishes incorrect signal associations, and the stack improves the signal-to-noise ratio, thereby lowering the detection threshold. Precision adjustments to the algorithm's parameters can produce robust recovery of lower magnitude events, along with an improved true-to-false ratio, therefore reducing the number of manual inspections required. Calculation time mainly rests upon the number of model grid points, but adequate spatial resolutions can be obtained within acceptable run-times (near real-time) using iterative up sampling. Migration-based event detection proves particularly appealing for studying natural or induced earthquake swarms or for monitoring areas of significant seismic activity that demonstrate low magnitude seismicity.

The described algorithm recovered 94 percent of genuine events by the system detection software and roughly doubled the overall count of authentically detected events. The percentage of false events declined from 40 percent to 25 percent even prior to the implementation of event selection criteria. Hypocentre estimations from our automatically detected events closely resemble events located with manually picked arrivals, with variances proportional to the size of the grid cell utilized. The attribute functions assessed produced matching overall detection statistics, with the Kurtosis function generating marginally fewer missed and false events. It is still mandatory to apply the appropriate pre-processing based on each type of attribute function.

Declaration of competing interest

The authors declare that they have no known competing financial interests or personal relationships that could have appeared to influence the work reported in this paper.

Author agreement and acknowledgment

The data used in this study are provided by the open source.

REFERENCES

- [1] R. M. Allen and D. Melgar, "Earthquake early warning: Advances, scientific challenges, and societal needs," *Annu. Rev. Earth Planet. Sci.*, vol. 47, no. May, pp. 361–388, 2019, doi: 10.1146/annurev-earth-053018-060457.
- [2] N. Agarwal, I. Arora, H. Saini, and U. Sharma, "A Novel Approach for Earthquake Prediction Using Random Forest and Neural Networks," *EAI Endorsed Trans. Energy Web*, vol. 10, pp. 1–6, 2023, doi: 10.4108/EW.4329.
- [3] G. Wurman, R. M. Allen, and P. Lombard, "Toward earthquake early warning in northern California," *J. Geophys. Res. Solid Earth*, vol. 112, no. 8, pp. 1–19, 2007, doi: 10.1029/2006JB004830.
- [4] H. S. Kuyuk and O. Susumu, "Real-time classification of earthquake using deep learning," *Procedia Comput. Sci.*, vol. 140, no. November, pp. 298–305, 2018, doi: 10.1016/j.procs.2018.10.316.
- [5] G. Yang, M. Zeng, X. Lin, S. Li, H. Yang, and L. Shen, "Real-time sharing algorithm of earthquake early warning data of hydropower station based on deep learning," *Earth Sci. Informatics*, no. 0123456789, 2024, doi: 10.1007/s12145-024-01400-9.
- [6] T. Bhardwaj, M. Kumar, and S. C. Sharma, "Megh: A private cloud provisioning various IaaS and SaaS," in *Advances in Intelligent Systems and Computing*, 2018. doi: 10.1007/978-981-10-5699-4_45.
- [7] P. Kumar, N. Zaidi, and T. Choudhury, "Fog computing: Common security issues and proposed countermeasures," in *Proceedings of the 5th International Conference on System Modeling and Advancement in Research Trends, SMART 2016*, 2017. doi: 10.1109/SYSMART.2016.7894541.
- [8] S. Chouliaras and S. Sotiriadis, "Auto-scaling containerized cloud applications: A workload-driven approach," *Simul. Model. Pract. Theory*, vol. 121, no. May, p. 102654, 2022, doi: 10.1016/j.simpat.2022.102654.
- [9] V. L. Padma Latha, N. Sudhakar Reddy, and A. Suresh Babu, "Optimizing Scalability and Availability of Cloud Based Software Services Using Modified Scale Rate Limiting Algorithm," *Theor. Comput. Sci.*, vol. 943, pp. 230–240, 2023, doi: 10.1016/j.tcs.2022.07.019.
- [10] G. Iannaccone *et al.*, "A prototype system for earthquake early-warning and alert management in southern

- Italy," *Bull. Earthq. Eng.*, vol. 8, no. 5, pp. 1105–1129, 2010, doi: 10.1007/s10518-009-9131-8.
- [11] Y.-W. Kwon, J.-K. Ahn, J. Lee, and C.-H. Lee, "EARTHQUAKE EARLY WARNING USING LOW-COST MEMS SENSORS", doi: 10.1109/IGARSS39084.2020.9323438.
- [12] Ö. Kafadar, S. Tunç, and B. Tunç, "ESenTRY: an on-site earthquake early warning system based on the instrumental modified Mercalli intensity," *Earth Sci. Informatics*, no. 1988, 2024, doi: 10.1007/s12145-024-01407-2.
- [13] Z. E. Ross, M. A. Meier, and E. Hauksson, "P Wave Arrival Picking and First-Motion Polarity Determination With Deep Learning," *J. Geophys. Res. Solid Earth*, vol. 123, no. 6, pp. 5120–5129, Jun. 2018, doi: 10.1029/2017JB015251.
- [14] G. Hloupis and F. Vallianatos, "Wavelet-Based Methods for Rapid Calculations of Magnitude and Epicentral Distance: An Application to Earthquake Early Warning System," *Pure Appl. Geophys.*, vol. 172, no. 9, pp. 2371–2386, 2015, doi: 10.1007/s00024-015-1081-2.
- [15] J. A. Khan, M. A. Z. Raja, M. I. Syam, S. A. K. Tanoli, and S. E. Awan, "Design and application of nature inspired computing approach for nonlinear stiff oscillatory problems," *Neural Comput. Appl.*, vol. 26, no. 7, pp. 1763–1780, 2015, doi: 10.1007/s00521-015-1841-z.
- [16] T. Perol, M. Gharbi, and M. Denolle, "Convolutional neural network for earthquake detection and location," *Sci. Adv.*, vol. 4, no. 2, pp. 2–9, 2018, doi: 10.1126/sciadv.1700578.
- [17] G. Joshi, R. Natsuaki, and A. Hirose, "Multi-Sensor Satellite-Imaging Data Fusion for Earthquake Damage Assessment and the Significant Features," *Proc. - 2021 7th Asia-Pacific Conf. Synth. Aperture Radar, APSAR 2021*, pp. 1–6, 2021, doi: 10.1109/APSAR52370.2021.9688438.
- [18] H. Kanamori, "Real-time seismology and earthquake damage mitigation," *Annu. Rev. Earth Planet. Sci.*, vol. 33, pp. 195–214, 2005, doi: 10.1146/annurev.earth.33.092203.122626.
- [19] P. Pierleoni, A. Belli, M. Esposito, R. Concetti, and L. Palma, "Earthquake Early Warning Services Based on Very Low-Cost Internet of Things Devices," *2022 61st FITCE Int. Congr. Futur. Telecommun. Infrastruct. Sustain. FITCE 2022*, no. Dii, pp. 1–5, 2022, doi: 10.23919/FITCE56290.2022.9934792.
- [20] I. W. Mustika, H. N. Adi, and F. Najib, "Comparison of Keras Optimizers for Earthquake Signal Classification Based on Deep Neural Networks," *ICOIACT 2021 - 4th Int. Conf. Inf. Commun. Technol. Role AI Heal. Soc. Revolut. Turbul. Era*, pp. 304–308, 2021, doi: 10.1109/ICOIACT53268.2021.9563990.
- [21] Z. Li, "Recent advances in earthquake monitoring i: Ongoing revolution of seismic instrumentation," *Earthq. Sci.*, vol. 34, no. 2, pp. 177–188, 2021, doi: 10.29382/eqs-2021-0011.
- [22] J. Seo, Y. Kim, J. Ha, D. Kwak, M. Ko, and M. Yoo, "Unsupervised anomaly detection for earthquake detection on Korea high-speed trains using autoencoder-based deep learning models," *Sci. Rep.*, vol. 14, no. 1, pp. 1–15, 2024, doi: 10.1038/s41598-024-51354-7.
- [23] K. A. Porter, J. L. Beck, and R. Shaikhutdinov, "Simplified estimation of economic seismic risk for buildings," *Earthq. Spectra*, vol. 20, no. 4, pp. 1239–1263, 2004, doi: 10.1193/1.1809129.
- [24] N. V. Chawla, K. W. Bowyer, L. O. Hall, and W. P. Kegelmeyer, "SMOTE: Synthetic Minority Over-sampling Technique," 2002.
- [25] S. Shadravan, H. R. Naji, and V. K. Bardsiri, "The Sailfish Optimizer: A novel nature-inspired metaheuristic algorithm for solving constrained engineering optimization problems," *Eng. Appl. Artif. Intell.*, 2019, doi: 10.1016/j.engappai.2019.01.001.
- [26] T. Feng, S. Mohanna, and L. Meng, "EdgePhase: A Deep Learning Model for Multi-Station Seismic Phase Picking," *Geochemistry, Geophys. Geosystems*, vol. 23, no. 11, Nov. 2022, doi: 10.1029/2022GC010453.
- [27] J. B. Rundle, A. Donnellan, G. Fox, and J. P. Crutchfield, "Nowcasting Earthquakes by Visualizing the Earthquake Cycle with Machine Learning: A Comparison of Two Methods," *Surveys in Geophysics*, vol. 43, no. 2. Springer Science and Business Media B.V., pp. 483–501, Apr. 01, 2022. doi: 10.1007/s10712-021-09655-3.
- [28] M. Saraswathi and T. Bhuvaneswari, "Multitenancy in Cloud Software as a Service Application," *Int. J. Adv. Res. Comput. Sci. Softw. Eng.*, 2013.
- [29] C. Peng *et al.*, "Performance Evaluation of an Earthquake Early Warning System in the 2019–2020 M6.0 Changning, Sichuan, China, Seismic Sequence," *Front. Earth Sci.*, vol. 9, Jul. 2021, doi: 10.3389/feart.2021.699941.

- [30] P. Jiao and A. H. Alavi, "Artificial intelligence in seismology: Advent, performance and future trends," *Geosci. Front.*, vol. 11, no. 3, pp. 739–744, 2020, doi: 10.1016/j.gsf.2019.10.004.
- [31] Y. Kodera *et al.*, "Developments of the Nationwide Earthquake Early Warning System in Japan After the 2011 Mw9.0 Tohoku-Oki Earthquake," *Front. Earth Sci.*, vol. 9, no. October, pp. 1–13, 2021, doi: 10.3389/feart.2021.726045.
- [32] H. S. Kuyuk, R. M. Allen, H. Brown, M. Hellweg, I. Henson, and D. Neuhauser, "Designing a network-based earthquake early warning algorithm for California: ElarmS-2," *Bull. Seismol. Soc. Am.*, vol. 104, no. 1, pp. 162–173, 2014, doi: 10.1785/0120130146.
- [33] F. Ismail, H. Mohamed Abdel-Kader, and M. Sami Soliman, "A new distributed earthquake early warning communication protocol based on messaging," 2022, doi: 10.21203/rs.3.rs-2033467/v1.
- [34] M. Böse, E. Hauksson, K. Solanki, H. Kanamori, and T. H. Heaton, "Real-time testing of the on-site warning algorithm in southern California and its performance during the July 29 2008 Mw5.4 Chino Hills earthquake," *Geophys. Res. Lett.*, vol. 36, no. 5, Mar. 2009, doi: 10.1029/2008GL036366.
- [35] L. R. Jaroszewicz, M. Dudek, A. T. Kurzych, and K. P. Teisseyre, "A test performance of optical fibre sensors for real-time investigations of rotational seismic events: a case study in laboratory and field conditions," *Opto-Electronics Rev.*, vol. 29, no. 4, pp. 213–219, 2021, doi: 10.24425/opelre.2021.140102.
- [36] J. Li *et al.*, "A real-time AI-assisted seismic monitoring system based on new nodal stations with 4G telemetry and its application in the Yangbi MS 6.4 aftershock monitoring in southwest China," *Earthq. Res. Adv.*, vol. 2, no. 2, p. 100033, 2022, doi: 10.1016/j.eqrea.2021.100033.
- [37] A. Chitkeshwar, "The Role of Machine Learning in Earthquake Seismology: A Review," *Arch. Comput. Methods Eng.*, no. 0123456789, 2024, doi: 10.1007/s11831-024-10099-2.
- [38] V. F. Grasso, J. L. Beck, and G. Manfredi, "Automated decision procedure for earthquake early warning," *Eng. Struct.*, vol. 29, no. 12, pp. 3455–3463, 2007, doi: 10.1016/j.engstruct.2007.08.020.
- [39] K. Pitilakis *et al.*, "Structural monitoring and earthquake early warning systems for the AHEPA hospital in Thessaloniki," *Bull. Earthq. Eng.*, vol. 14, no. 9, pp. 2543–2563, 2016, doi: 10.1007/s10518-016-9916-5.